Numerical Analysis of a TM_{010} Cavity for Dielectric Measurement

Xiaolu Zhao, Ce Liu, *Member, IEEE,* and Liang C. Shen, *Fellow IEEE*

Abstract—**The property of a TM_{010} cavity containing a lossy dielectric material is obtained by using the transmission-line-matrix (TLM) technique with serial nodes in cylindrical coordinates. The TM_{010} cavity operating at 1.1 GHz has three concentric layers and an air gap between the sample and cavity cover. The influence of this air gap in terms of the Q-factor and the resonant frequency is studied by the numerical method. Employing the serial graded TLM technique, the resonant curve of the cavity is computed. From this, the Q factor and the center frequency can be evaluated. In the TLM method, the entire cavity space is discretized into small cells. Maxwell's equations in each cell are transformed into a matrix of transmission line equations. The voltage and the current in the inter-connected transmission line network are proportional to the electric and the magnetic field. The formulation of the method is in cylindrical coordinates and each cell may have different physical dimensions. Compared with the TLM method in rectangular coordinates and uniform grids, the present method is more efficient and easier to program for the analysis of the cavity with cylindrical symmetry. Computed results show that the air gap between the sample and cavity cover is very critical to the accuracy of the measurement of the dielectric property of the sample when the sample diameter is small, but negligible when the diameter of the sample is large.**

Introduction

THE MEASUREMENT of the conductivity σ and the relative dielectric permittivity ϵ_r at ultra-high frequency for highly lossy materials is important for many industrial applications [1]–[5]. Unfortunately, many measurement setups are not totally accurate because of the high conductivity of the material. One of the useful methods is the TM_{010} cavity measurement system which uses a very thin sample holder at the center of the cavity [3], [4] within which a lossy sample is placed. This system has the advantage of allowing the sample temperature and sample pressure to be easily controlled. Since the sample holder is thin and filled with highly conductive material, an air gap between the sample and the cavity cover may have an important effect on the accuracy of the measurement. Understanding the degree of influence of the air gap is essential to the interpretation of measured data. Analytic and perturbation solutions are not available for the case when the air gap exists [3]. In the discussion to follow, the center frequency of the cavity is set at about 1.1 GHz. The reason for this frequency choice is that 1.1 GHz is the operating frequency of a recent developed dielectric well logging tool.

The transmission line matrix (TLM) method is used in this paper to study the effect of the air gap. The TLM method in rectangular coordinates is discussed in [6]–[8]. A summary paper was published by Hoefer [9]. Detailed applications and properties of the TLM method are also illustrated by Hoefer in [10]. Al-Mukhtar and Sitch [11] discussed the two-dimensional TLM method in polar coordinates ($r - \theta$ system). In the case of cylindrical coordinates with axial symmetry ($r - z$ system), a paper was published by Liu and Shen [12] discussing TLM method for TE modes. In regard to TE modes, a shunt TLM node is used to simulate the Maxwell's equations. The energy loss due to the conductivity of the sample is directly related to the E field in the cavity. Since voltages at the TLM nodes are used to simulate the E field, conductivity of the sample is included in the scattering matrix of each node without changing the scattering process. When TM mode is assumed in the computation, serial nodes are used. Consequently, conductivity can not be included in the scattering matrix of the node which describes the interaction between H fields. The energy loss due to the conductivity of the sample has to be taken account by an additional shunt node which is connected to adjacent serial nodes. Thus, a serial-shunt nodes structure is used for the simulation of Maxwell's equations in the TM mode. This TLM structure results in the change of the algorithm described in [12]. In each iteration, two scattering processes are involved. One is at the serial nodes and the other at the shunt nodes.

Maxwell and Transmission Line Equations

A cylindrical TM_{010} resonant cavity for the measurement of the complex dielectric constant of lossy materials is shown in Fig. 1. The system is axially symmetrical. The sample holder, which is usually made of plexiglass, is located at the center of the cavity. Samples are machined to cylinders and placed into the sample holder. The central part of the upper cover of the cavity is removable to allow ease of sample installment. It is quite possible in the practical operation that a small gap exists between the sample and the cavity cover.

The fields in the cavity are only functions of r and z

Manuscript received March 6, 1991; revised March 12, 1992.

X. Zhao is with OYO Geospace, 7334 N. Gessener, Houston, TX 77040.
C. Liu and L. C. Shen are with the Department of Electrical Engineering, University of Houston, Houston, TX 77204-4793.

IEEE Log Number 9202137.

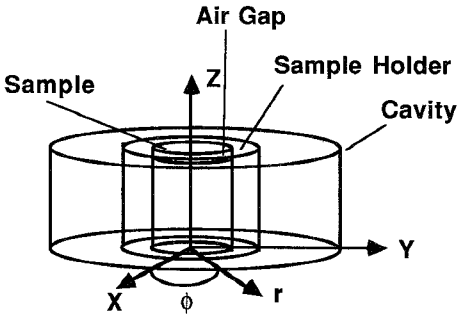

Fig. 1. The TM_{010} resonant cavity for dielectric measurements.

since axial symmetry is maintained in the system. The Maxwell's equations for TM mode inside the cavity with the assumption of axial symmetry are as follows:

$$\frac{\partial H_\phi}{\partial z} = -\epsilon \frac{\partial E_r}{\partial t} - \sigma E_r \tag{1}$$

$$\frac{1}{r}\frac{\partial (rH_\phi)}{\partial r} = \epsilon \frac{\partial E_z}{\partial t} + \sigma E_z \tag{2}$$

$$\frac{\partial E_r}{\partial z} - \frac{\partial E_z}{\partial r} = -\mu \frac{\partial H_\phi}{\partial t} \tag{3}$$

where, ϵ, σ and μ are dielectric permittivity, electric conductivity, and magnetic permeability of the medium, respectively.

Since the present problem is two-dimensional, like the finite difference method, we first divide the area of interest into small cells, as shown in Fig. 2. Each cell has a length of Δr in the r direction and Δz in the z direction. Δr and Δz may be different in length from cell to cell. The electromagnetic fields in each cell satisfy Maxwell's equations (1)–(3).

To simulate Maxwell's equations in each cell shown in Fig. 2, a transmission line node is placed in the cell. Each node has five interconnected transmission lines. Each arm of the linking line to the next node is connected to a shunt node. At this point, a conductance is connected in parallel. Because the conductive loss is related to the E-field [(1) and (2)], the simulation of these two equations with transmission line node must have a common voltage. This means a shunt node has to be used. Therefore, the conductance located at the TLM shunt node as shown in Fig. 3(a) is separated from the serial node by a time delay of $\tau/2$ as shown in Fig. 3(b). The serial connected lines simulate (3) and the others simulate (1) and (2). The current and voltage equations in the TLM node are as follows:

$$\Delta z \frac{\partial I_\phi}{\partial z} = C_z \frac{\partial V_r}{\partial t} + G_z V_r \tag{4}$$

$$\Delta r \frac{\partial I_\phi}{\partial r} = C_r \frac{\partial V_z}{\partial t} + G_r V_z \tag{5}$$

$$-\Delta z \frac{\partial V_r}{\partial z} - \Delta r \frac{\partial V_z}{\partial r} = -L_{rz} \frac{\partial I_\phi}{\partial t} \tag{6}$$

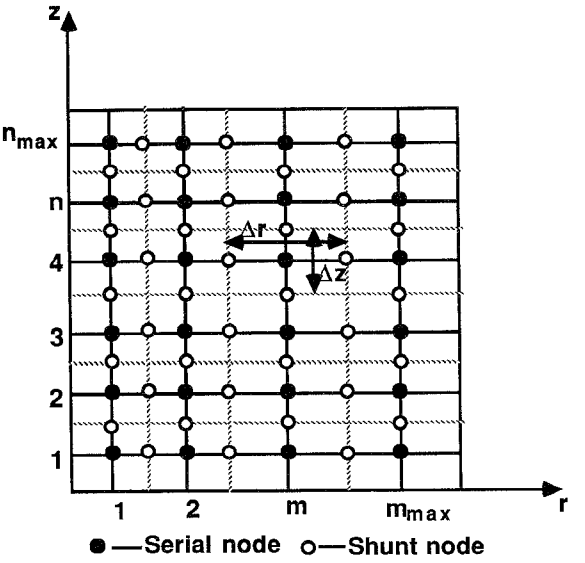

Fig. 2. The transmission line matrix in cavity space.

where C_r and C_z are shunt capacitances in farads in z and r directions respectively, G_r and G_z are shunt conductances in mhos in r and z directions, respectively, and L_{rz} is the total inductance of the node in henrys. Define

$$I_\phi = rH_\phi \tag{7}$$

$$V_z = \Delta z E_z \tag{8}$$

$$V_r = -\Delta r E_r \tag{9}$$

$$C_r = \frac{\epsilon r \Delta r}{\Delta z} \tag{10}$$

$$C_z = \frac{\epsilon r \Delta z}{\Delta r} \tag{11}$$

$$G_r = \frac{\sigma r \Delta r}{\Delta z} \tag{12}$$

$$G_z = \frac{\sigma r \Delta z}{\Delta r} \tag{13}$$

$$L_{zr} = \frac{\mu \Delta r \Delta z}{r}. \tag{14}$$

Direct substitution of the above relations to (4)–(6) gives Maxwell's equations (1)–(3).

Throughout this procedure, the propagation of current and voltage in the transmission line matrix shown in Fig. 3 is equivalent to the propagation of the TM wave in an axially symmetrical space shown in Fig. 1.

The Transmission Line Matrix

In evaluating the scattering matrix, the characteristic impedance of each line must be known. Furthermore, the propagation speed of current and voltage on each section of the transmission line matrix must be kept the same so that the iteration process is synchronized. Note that (10)–

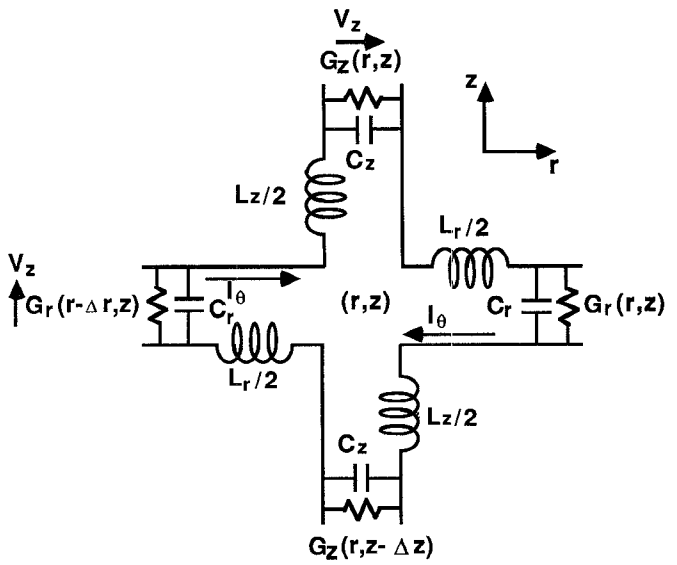

(a)

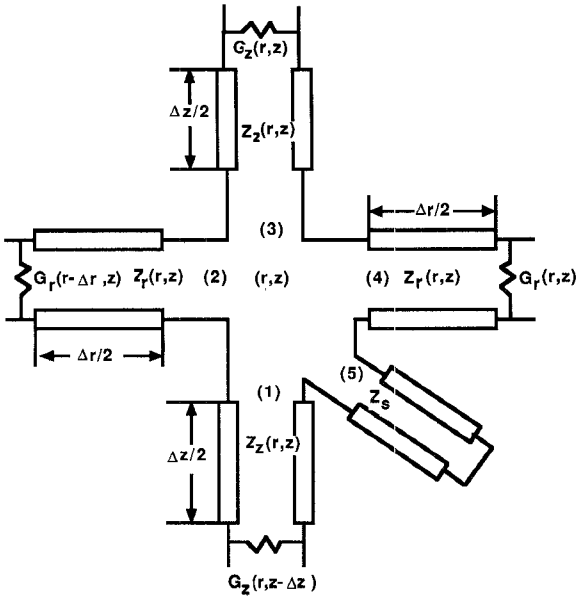

(b)

Fig. 3. (a) The lumped equivalent circuit of a serial TLM unit. (b) The serial transmission line unit.

(13) define capacitance and conductance of each transmission line node. But in (14), only total inductance L_{zr} is specified. L_r and L_z are allowed to be adjusted individually to maintain time synchronization.

Let total serial inductance of the node be the sum of L_z and L_r plus a residual inductor with inductance L_s,

$$L_{zr} = L_z + L_r + L_s. \tag{15}$$

The propagation time from one node to the next in r and z direction is given as follows:

$$\tau_r = \sqrt{L_r C_r} \tag{16}$$

$$\tau_z = \sqrt{L_z C_z} \tag{17}$$

To maintain time synchronization, τ_r and τ_z must be equal. Let

$$\tau_r = \tau_r = \tau = h\sqrt{\mu_0 \epsilon_0} \tag{18}$$

where h is a constant to be determined later. From (18) and (10) and (11), L_z and L_r can be found to be

$$L_r = \frac{h^2 \mu_0 \Delta z}{r \Delta r \epsilon_r} \tag{19}$$

$$L_z = \frac{h^2 \mu_0 \Delta r}{r \Delta z \epsilon_r}. \tag{20}$$

Therefore, the residual inductor of the node is found by substituting (19) and (20) to (15) and (14):

$$L_s = \frac{\mu_0}{r}\left(\Delta r \Delta z - h^2 \frac{\Delta r}{\epsilon_r \Delta z} - h^2 \frac{\Delta z}{\epsilon_r \Delta r}\right). \tag{21}$$

The condition for (21) to be valid is that L_s must be positive or zero, which leads to the following equation:

$$h^2 = \text{Min}\left(\frac{\Delta r \Delta z \epsilon_r}{\frac{\Delta r}{\Delta z} + \frac{\Delta z}{\Delta r}}\right) \tag{22}$$

where Min [·] means the minimum of the argument value in the entire region of interest.

Since the inductance and capacitance of the lines in z and r directions have now been determined, characteristic impedances of these lines are given by the following equations:

$$Z_r = \frac{\Delta z h}{\Delta r \epsilon_r r}\sqrt{\frac{\mu_0}{\epsilon_0}} \tag{23}$$

$$Z_z = \frac{\Delta r h}{\Delta z \epsilon_r r}\sqrt{\frac{\mu_0}{\epsilon_0}}. \tag{24}$$

A residual inductance is introduced to maintain the time synchronization. The residual inductance is simulated by a section of short-circuited transmission line under long wavelength assumption [11]. The impedance of the stub can be found to be

$$Z_s = \frac{2}{rh}\sqrt{\frac{\mu_0}{\epsilon_0}}\left(\Delta r \Delta z - h^2 \frac{\Delta r}{\epsilon_r \Delta z} - h^2 \frac{\Delta z}{\epsilon_r \Delta r}\right). \tag{25}$$

Infinitive long transmission lines may simulate the conductances [9]–[11]. The input admittances, which are also characteristic admittances, are just equal to those of the conductors. That is:

$$Y_r = G_r = \frac{r \Delta r \sigma}{\Delta z} \tag{26}$$

$$Y_z = G_z = \frac{r \Delta z \sigma}{\Delta r}. \tag{27}$$

With these parameters, the scattering matrix of the serial node can be found to be

$$[s] = \frac{2}{Z}\begin{pmatrix} Z_r & Z_z & Z_z & -Z_z & -Z_z \\ Z_r & Z_z & -Z_r & Z_r & Z_r \\ Z_z & -Z_z & Z_r & Z_z & Z_z \\ -Z_r & Z_r & Z_r & Z_z & -Z_r \\ -Z_s & Z_s & Z_s & -Z_s & -Z_s + Z_r + Z_z \end{pmatrix} + \frac{Z_s}{Z}[I] \tag{28}$$

where $Z = 2Z_z + 2Z_r + Z_s$ and [I] is a 5×5 unit matrix. This scattering matrix links the reflected wave and the incident wave by the following relations:

$$\begin{pmatrix} V_{r1} \\ V_{r2} \\ V_{r3} \\ V_{r4} \\ V_{r5} \end{pmatrix} = \begin{pmatrix} s_{11} & s_{12} & s_{13} & s_{14} & s_{15} \\ s_{21} & s_{22} & s_{23} & s_{24} & s_{25} \\ s_{31} & s_{32} & s_{33} & s_{34} & s_{35} \\ s_{41} & s_{42} & s_{43} & s_{44} & s_{45} \\ s_{51} & s_{52} & s_{53} & s_{54} & s_{55} \end{pmatrix} \begin{pmatrix} V_{i1} \\ V_{i2} \\ V_{i3} \\ V_{i4} \\ V_{i5} \end{pmatrix} \tag{29}$$

where $V_{ij}(j = 1, 5)$ and $V_{rj}(j = 1, 5)$ are respectively the incident and reflect voltages at port j, where j is local coding of the serial transmission line node defined in Fig. 3(b).

At the shunt node, the scattering matrix is a 2×2 matrix. As shown in Figs. 4 and 5, reflection appears not only because of different impedances of the transmission line segments from node to node, but also the existence of the conductance G_r and G_z. In r direction, as shown in Fig. 4, the scattering matrix can be determined as follows:

$$s_{11} = \frac{Y_r(r - \Delta r, z) - [G_r(r, z) + Y_r(r, z)]}{Y_r(r - \Delta r, z) + G_r(r, z) + Y_r(r, z)} \tag{30}$$

$$s_{22} = \frac{Y_r(r, z) - [G_r(r, z) + Y_r(r - \Delta r, z)]}{Y_r(r - \Delta r, z) + G_r(r, z) + Y_r(r, z)} \tag{31}$$

$$s_{12} = 1 + s_{22} \tag{32}$$

$$s_{21} = 1 + s_{11} \tag{33}$$

where $Y_z = 1/Z_z$ and $Y_r = 1/Z_r$.

With the local coding of shunt transmission line node defined as shown in Figs. 4 and 5 for r direction and z direction respectively, the reflected and the incident voltage at the shunt node are related by the scattering matrix as

$$\begin{pmatrix} V_{1r}(r, z) \\ V_{2r}(r, z) \end{pmatrix} = \begin{pmatrix} s_{11} & s_{12} \\ s_{21} & s_{22} \end{pmatrix} \begin{pmatrix} V_{1i}(r, z) \\ V_{2i}(r, z) \end{pmatrix}. \tag{34}$$

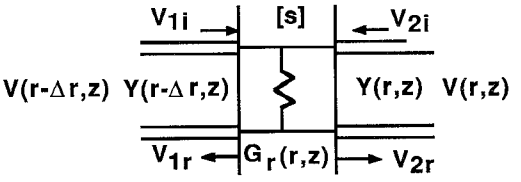

Fig. 4. The scattering matrix at a shunt node (r direction).

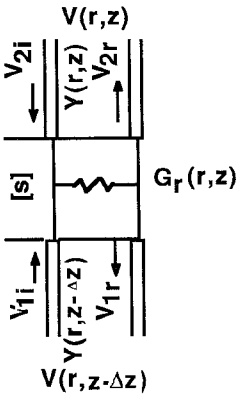

Fig. 5. The scattering matrix at a shunt node (z direction).

Similarly, in the z direction, the elements of the scattering matrix are as follows:

$$s_{11} = \frac{Y_z(r, z - \Delta z) - [G_z(r, z) + Y_z(r, z)]}{Y_z(r, z - \Delta z) + G_z(r, z) + Y_z(r, z)} \tag{35}$$

$$s_{22} = \frac{Y_z(r, z) - [G_z(r, z) + Y_z(r, z - \Delta z)]}{Y_z(r, z - \Delta z) + G_z(r, z) + Y_z(r, z)} \tag{36}$$

$$s_{12} = 1 + s_{22} \tag{37}$$

$$s_{21} = 1 + s_{11}. \tag{38}$$

With the local coding of the port at the shunt node defined in Fig. 5, the incident and the reflected node voltages are related by the following equation:

$$\begin{pmatrix} V_{1r}(r, z) \\ V_{2r}(r, z) \end{pmatrix} = \begin{pmatrix} s_{11} & s_{12} \\ s_{21} & s_{22} \end{pmatrix} \begin{pmatrix} V_{1i}(r, z) \\ V_{2i}(r, z) \end{pmatrix}. \tag{39}$$

Since the system is axially symmetrical, the axis of the cylinder is a symmetrical boundary. The iteration equation at these nodes can be written as

$$V_{\text{in}}(\Delta r/2, z, t + \Delta t) = V_r(\Delta r/2, z, t). \tag{40}$$

The cavity is assumed to be made of a perfect conductor. The boundaries formed by the walls of the cavity are simulated by short-circuited transmission lines. There are three boundaries which belong to this kind of short-circuited stub: upper cover, bottom, and the side wall of the cavity. At the upper cover, the iteration equation is given as follows:

$$V_{\text{in}}(r, W - \Delta W/2, t + \Delta t) = -V_r(r, W - \Delta W/2, t) \tag{41}$$

where W is the height of the cavity and ΔW is the grid length at the boundary in the z direction.

Similarly, at the bottom and the wall of the cavity, the iteration equations are as follows:

$$V_{in}(r, \Delta z/2, t + \Delta t) = -V_r(r, \Delta z/2, t) \quad (42)$$

$$V_{in}(R - \Delta R/2, z, t + \Delta t) = -V_r(R - \Delta R/2, z, t) \quad (43)$$

where R is the radius of the cavity and ΔR is the grid length at the cavity wall in the r direction.

Verification of the Numerical Analysis

The empty cavity is used for basic verification of the numerical method. Nonuniform grid is chosen. With different grids show in Fig. 6, for different number of iteration, the computed resonant frequency is compared with the theoretical values given in [13]. Table I shows the comparison of center frequency computed with TLM technique and the analytical result. In Table I(a), where nodes are non-uniformly graded in the z direction, uniform grids are applied in r direction. When the number of iterations is greater than 1000, the relative error which is defined as $(f_{tlm} - f_{\text{theory}})/f_{\text{theory}}$ is less than 0.5 percent. When the number of iterations increases, the error monotonically decreases; which reflects good convergence property of the method. Table I(b) also shows similar results when the cavity space is non-uniformity graded in the r direction.

Another verification is done when the cavity is loaded with a cylindrical sample of lossless material as shown in Fig. 7. Table II shows the computed data and comparison with measured data. This illustrates that the TLM computation has a satisfactory accuracy level.

When the entire cavity is filled with lossy uniform material, analytic solution for the Q factor and center frequency can be found [13]. The computed data with TLM technique in these cases is compared with the analytical solution as shown in Table III. In this case, the number of iteration is greatly increased to achieve a satisfactory accuracy for Q factor. Resonant frequency is determined by the center of the resonant curve, while the Q factor is determined by the shape of the resonant curve. Compared with resonant frequency, the Q factor needs more iteration to achieve the same accuracy. Physically, this may be explained as follows: when conductivity is presented in the system, fields are influenced by low frequency components. To take this portion of fields into account, the contribution from low frequency components has to be computed, this implies that a wider time window in the time domain must be chosen.

Tables I–III clearly show that the TLM computation for the structure with cylindrical symmetry is reasonably accurate when the proper number of iterations is selected.

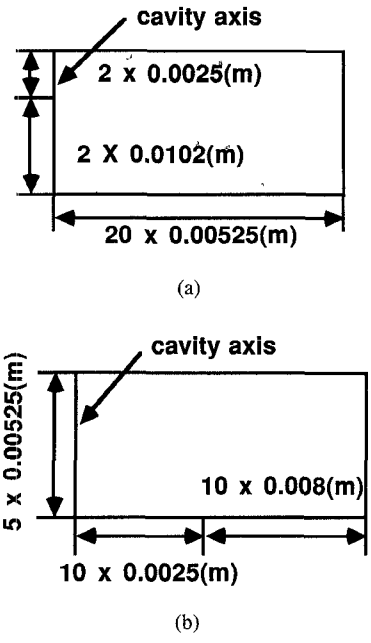

Fig. 6. (a) The cavity space is divided into non-uniform grids in z direction and uniform grids in r direction. (b) The cavity space is divided into nonuniform grids in r direction and uniform grids in z direction.

TABLE I
COMPARISON OF RESONANT FREQUENCY OF AN AIR FILLED TM_{010} CAVITY COMPUTED BY TLM METHOD USING TWO DIFFERENT GRIDS WITH THEORETICAL VALUES

(a) Nonuniform Grids in z Direction [Fig. 6(a)]

Iteration	1000	2000	3000	5000	Theory
F_0 (MHz)	1088.3	1090.6	1091.1	1091.5	1093.6
Error	−0.48%	−0.27%	−0.23%	−0.19%	

(b) Nonuniform Grids in r Direction [Fig. 6(b)]

Iteration	2000	3000	5000	10000	Theory
F_0 (MHz)	1085.3	1088.3	1088.9	1089.1	1093.6
Error	0.76%	−0.48%	−0.43%	−0.41%	

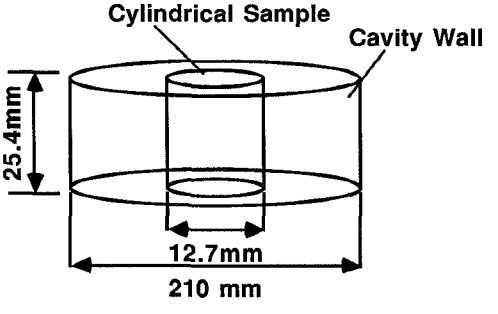

Fig. 7. A lossless sample is placed in the cavity. The set-up is used to verify the TLM method.

TABLE II
COMPARISON OF THE COMPUTED DATA WITH MEASURED DATA FOR THREE DIFFERENT SAMPLES

	Plexiglas $\epsilon_r = 2.69$	Nylon $\epsilon_r = 3.04$	Teflon $\epsilon_r = 2.05$
F_0 (MHz) Measured	1079.37	1076.70	1084.16
F_0 (MHz) TLM	1078.80	1076.00	1083.70

TABLE III
COMPARISON OF Q FACTOR COMPUTED BY TLM METHOD WITH THEORETICAL DATA. THE CAVITY IS UNIFORMLY FILLED WITH A LOSSY MATERIAL WITH $\epsilon_r = 1$ AND $\sigma = 0.001$

(a) Nonuniform Grids in z Direction [Fig. 6(a)]

Iteration	7500	10000	15000	Theory
F_0 (MHz)				1093 6
Q	54.03	58.21	60.47	60.81
Q Error	−11.1%	−4.3%	−0.56%	

(b) Nonuniform Grids in r Direction [Fig. 6(b)]

Iteration	7500	10000	15000	Theory
F_0 (MHz)				1093 6
Q	51.83	57.91	60.48	60.81
Q Error	−14.8%	−4.8%	−0.54%	

THE INFLUENCE OF AIR GAP

To study the influence of an air gap on the measurement accuracy, a numerical model is shown in Fig. 8, in practical measurements, it is assumed that the sample is perfectly connected to the cavity cover. Interpretation of the measured data is carried out accordingly. Existence of the air gap between the lossy sample and the cavity cover is likely in practical measurements. Therefore, the error introduced by the air gap must be accounted for if the effect is significant.

From a physical point of view, the air gap cuts off the conductive current connecting the sample to the cavity cover. To maintain current continuation, displacement current is set up inside the gap. From the circuit point of view, a capacitance between the upper surface of the sample and the cavity cover is formed providing a path for displacement current to flow. It is apparent that the degree of influence due to the air gap on the dielectric measurement depends not only on the conductivity of the sample and the size of the gap, but also on the diameter of the sample. The sample diameter and the air gap determine the value of the capacitance.

Numerical computations are designed to investigate these influences on the measured center frequency and Q factor. Table IV enumerates the deviations from the values obtained when taking the data with no gap between sample and cavity cover as the base. The sample holder is assumed to be lossless with a dielectric constant of ϵ_0.

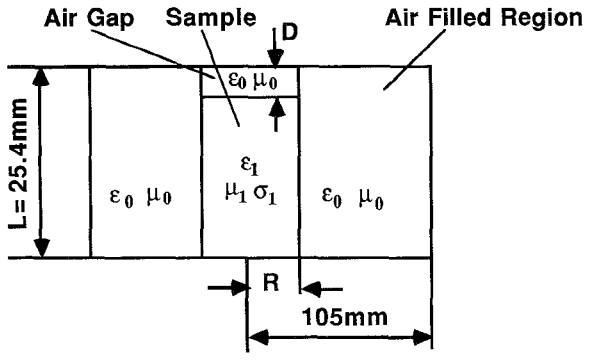

Fig. 8. The numerical model for the simulation of air gap between the sample and the upper cover of the cavity.

Theoretically, if there is no discontinuity in the structure, the change in Q factor is proportional to the change in volume of the sample. The data in Table IV(a) clearly show that with the air gap between the sample and cavity cover, the change in the Q factor of the cavity is greater than the change in the volume of the sample. Error in Q factor increases as the diameter of the sample decreases. A physical picture behind this phenomenon is that if the gap size is kept unchanged, as the diameter of the sample decreases, the value of the capacitance formed by the cavity cover and the top area of the sample decreases. This leads to less current flow in the lossy sample. Consequently, the increase in Q factor is greater than the decrease in volume of the sample. For example, when the gap is 1 mm wide, or 3.9% of the total length of the cavity, the change in the Q factor varies from 4.9% when the sample radius is 15.75 mm to 26.8% when the radius is 1 mm.

The change in the Q factor increases with the size of the gap. From Table IV(b), it is seen that errors in center frequency of the cavity due to the gap are negligible. For the same diameter of the sample, when the conductivity of the sample increases, the error due to the air gap increases greatly. This suggests that the discontinuity introduced by the air gap significantly cuts off the conducting current in the sample. Higher conductivity of the sample means stronger conducting current in the sample and hence is more affected by the presence of the gap. The capacitance coupling in the case of high sample conductivity couples less energy. Therefore, the error due to the air gap on the Q factor, which is inversely proportional to the energy loss in the cavity, will increase as the size of the air gap increases.

EXPERIMENT RESULTS

An experimental setup for the measurement of the electric properties of lossy materials was carried out. The TM_{010} cavity made of aluminum has a center frequency

TABLE IV (a)
INFLUENCE OF AN AIR GAP TO THE Q FACTOR OF THE CAVITY. PARAMETERS ARE GIGEN IN FIG. 8

		R = 1 00 mm ϵ_1 = 20.85 σ_1 = 3.225		R = 5.25 mm ϵ_1 = 1.72 σ_1 = 0.117		R = 10.50 mm ϵ_1 = 1.18 σ_1 = 0.029		R = 15.75 mm ϵ_1 = 1.08 σ_1 = 0.013	
D (mm)	D/L	Q	ΔQ (%)	Q	ΔQ (%)	Q	ΔQ (%)	Q	ΔQ (%)
0.0		52.9		53.8		55.2		56.6	
1.0	3.9%	67.1	26.8%	58.0	7.8%	58.0	5.1%	59.4	4.9%
2.0	7.9%	74.7	41.2%	62.0	15.2%	61.8	12.0%	62.0	9.5%
5.0	19.7%	93.8	77.3%	74.5	38.5%	72.3	31.0%	72.6	28.3%

TABLE IV (b)
INFLUENCE OF AN AIR GAP TO THE CENTER FREQUENCY OF THE CAVITY. PARAMETERS ARE GIVEN IN FIG. 8

D (mm)	R = 1.00 mm ϵ_1 = 20.85 σ_1 = 3.225	R = 5.25 mm ϵ_1 = 1.72 σ_1 = 0.117	R = 10.50 mm ϵ_1 = 1.18 σ_1 = 0.029	R = 15.75 mm ϵ_1 = 1.08 σ_1 = 0.013
0.0	1086.70	1087.45	1087.45	1087.45
1.0	1087.00	1087.45	1087.60	1087.75
2.0	1087.00	1087.60	1087.75	1087.75
5.0	1087.60	1087.90	1088.05	1088.30

TABLE V
COMPARISON OF MEASURED DATE WITH GOOD CONTECT AND WITHOUT CONTECT BETWEEN THE COVER AND THE SAMPLE. R IS THE RADIUS OF THE SAMPLE HOLDER
(The outer diameter of the sample holder is 6.35 mm)

		20 kppm R = 0.75 (mm)	13 kppm R = 1.0 (mm)	8 kppm R = 1.25 (mm)
Q	contact	68.9	55.8	51.3
	no contact	82.3	63.2	63.2
F (MHz)	contact	1071.82	1064.92	1055.40
	no contact	1071.20	1064.12	1054.81
	ΔQ	19.4%	13.3%	10.3%
	ΔF	0.06%	0.08%	0.06%

of 1093.6 MHz without the sample holder. Three sample holders with different inner diameters were used for different sample conductivities. At the center part of the upper cover of the cavity, a removable metal pin was mounted for making good connection with the sample. Current loops were used for the excitation and receiving of the signal. A HP-8505A Network Analyzer with a HP-8503A S-Parameter Test Set, and a HP-8501A Storage-Normalizer were used for the measurement. Temperature controller and heating devices were used for the measurement at different temperatures. The system was controlled by a HP-9000/216 computer.

Highly conductive saline solutions were used as samples. Three salinities of the solutions were used: 20 kppm, 13 kppm and 8 kppm. At room temperature, with and without contact to the upper cover of the cavity, the measured data agreed with the computed results, as shown in Table V.

Electrical properties of the highly conductive saline solutions at elevated temperatures were measured with this setup. Examples of the measured dielectric constant versus temperature are shown in Fig. 9 for the saline solutions with salinity of 5 kppm, 10 kppm, 15 kppm, and 20 kppm. Fig. 10 shows the measured conductivity of the saline solutions. At each temperature point, eight independent measurements were conduted and the average of the eight measurements are plotted. The measured data are compared with the empirical formula given by Saxton and Lane [2], [5] and the measured data by Han *et al.* [5].

CONCLUSIONS

The TLM method is useful in the analysis of TM_{010} resonant cavity for dielectric measurements. The air gap between the lossy sample and cavity cover plays an important role in determining the accuracy of the measurement. The error in the center frequency of the cavity due to the air gap is negligible. Error in the Q-factor due to

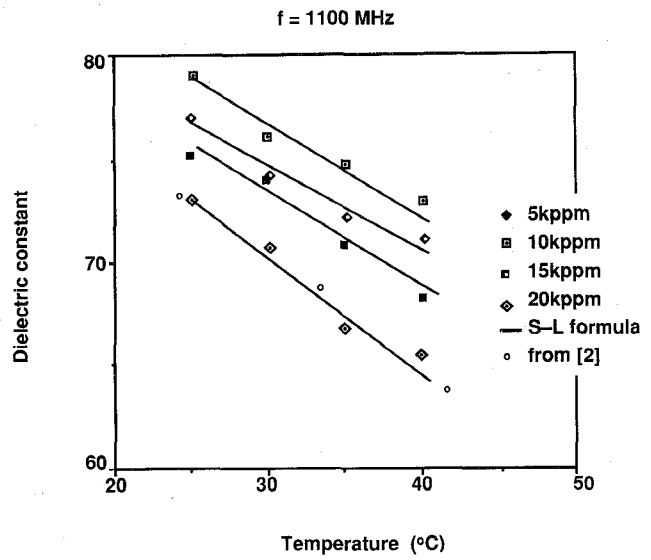

Fig. 9. Measured effective dielectric constant of saline solutions at elevated temperatures.

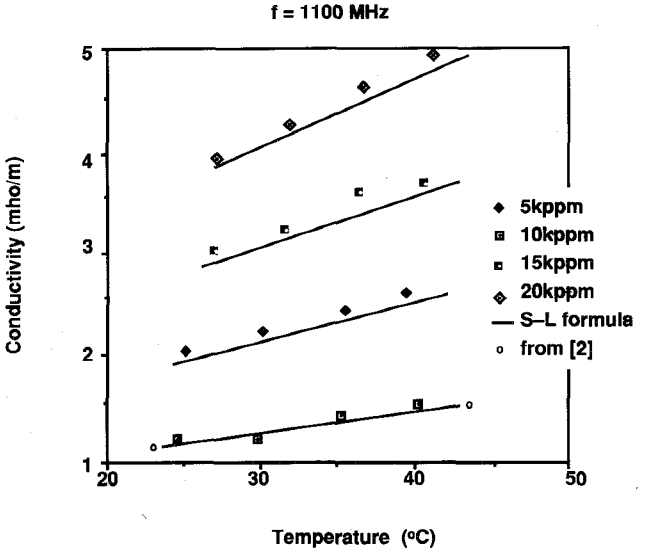

Fig. 10. Measured conductivity of saline solutions at elevated temperatures.

the air gap can be significant when the conductivity of the sample is high and the diameter of the sample is small. Unfortunately, in the case of a highly lossy sample, a small sample diameter must be used to maintain a reasonably high Q factor. Our analysis indicates that this is the worst case in terms of air gap influence. Special techniques, such as applying a connecting needle to the upper cover of the cavity, are recommended to minimize the error caused by the air gap.

ACKNOWLEDGMENT

The authors gratefully acknowledge the financial support and technical assistance given by the consoritum of 15 oil and service companies on this project.

REFERENCES

[1] L. C. Shen, "A laboratory technique for measuring dielectric properties of core samples at ultrahigh frequencies," *SPE J.*, pp. 502–514, Aug. 1985.

[2] K. F. Han, C. M. Butler, L. C. Shen, Y. D. He, and M. A. Haris, "High frequency, complex dielectric permittivity of saline solution at elevated temperatures," *IEEE Trans. Geosci. Remote Sensing*, vol. 29, no. 1, pp. 48–56, Jan. 1991.

[3] S. Li, C. Akyel, and R. G. Bosisio, "Precise calculations and measurements on the complex dielectric constant of lossy materials using TM_{010} cavity perturbation technique," *IEEE Trans. Microwave Theory Tech.*, vol. MTT-29, no. 10, pp. 1041–1047, Oct. 1981.

[4] M. Jaworski, "On the resonant frequency of a reentrant cylindrical cavity," *IEEE Trans. Microwave Theory Tech.*, vol. MTT-26, pp. 256–260, Apr. 1978.

[5] J. A. Saxton, and J. A. Lane, "Electrical properties of sea water," *Wireless Engineer*, pp. 269–275, Oct. 1952.

[6] P. B. Johns and R. L. Beurle, "Numerical solution of 2-dimensional scattering problems using a transmission-line matrix," *Proc. Inst. Elec. Eng.*, vol. 119, no. 8, pp. 1086–1091, Aug. 1972.

[7] S. Akhtarzad and P. B. Johns, "Numerical solution of lossy waveguide: T.L.M. computer program," *Electron. Lett.*, vol. 10, no. 15, pp. 309–311, July 25, 1974.

[8] ——, "Generalized Elements for T.L.M. Method of Numerical Analysis," *Proc. Inst. Elec. Eng.*, vol. 122, no. 12, pp. 1349–1352, Dec. 1975.

[9] W. J. R. Hoefer, "The transmission line matrix method-theory and applications," *IEEE Trans. Microwave Theory Tech.*, vol. 33, pp. 882–893, 1985.

[10] T. Itoh, *Numerical Techniques for Microwave and Millimeter-Wave Passive Structures*. New York: Wiley, 1988, ch. 8.

[11] D. A. Al-Mukhtar and J. E. Sitch, "Transmission-line matrix method with irregularly graded space," *Proc. Inst. Elec. Eng., Part H*, vol. 128, pp. 298–305, Dec. 1981.

[12] C. Liu and L. C. Shen, "Response of electromagnetic-pulse logging sonde in axially-symmetrically formation," *IEEE Trans. Geosci. Remote Sensing*, vol. 29, no. 2, pp. 214–221, Mar. 1991.

[13] R. E. Colin, *Field Theory of Guided Waves*. New York: McGraw-Hill, 1960.

Xiaolu Zhao was born on July 9, 1965 in Beijing China. He received the B.S. degree from Tsinghua University in 1987 and the M.S. degree from the University of Houston in 1991.

Mr. Zhao is currently with OYO Geospace.

Ce. Liu (M'90) received the B.S., M.S., and Ph.D. degrees from Xian Jiaotong University, Xian, P. R. China, in 1982, 1984, and 1988, respectively.

He joined the Department of Electrical Engineering at the University of Houston in 1988, and is now an Assistant Professor of the Department. Dr. Liu has worked on the research projects related to microwave passive and active networks, numerical simulation of electromagnetic scattering and propagation, hardware and software design of ground-penetrating radar systems, electromagnetic tomography, electrical properties of rocks, well logging, and physical modeling.

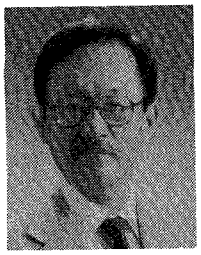

Liang C. Shen (S'65-M'67-SM'77-F'87) received the B.S.E.E. degree from the National Taiwan University in 1961 and the S. M. and the Ph.D. degrees in applied physics from Harvard University in 1963 and 1967 respectively.

He joined the faculty of the University of Houston in 1967 and is now a Professor in the Department of Electrical Engineering. He served as the Department Chairman from 1977 to 1981 and was a full-time research consultant at Gulf Oil Exploration and Production Company during 1981–82 and a Research Fellow at ARCO Oil and Gas Company during 1990–91. He is presently the Director of the Well Logging Laboratory at the University of Houston. His current interest is electromagnetic subsurface sensing, including electrical properties of rocks, well logging, physical modeling, environmental detection and monitoring, and subsurface tomography. Dr. Shen is a member of AGU, ASEE, Phi Tau Phi, SEG, Sigma Xi, SPE, SPWLA and URSI/USNC Commission B. He has served as a member of the Publication Committee of *The Log Analyst*, and an Associate Editor for *Geophysics*, *Radio Science*, and IEEE TRANSACTIONS ON GEOSCIENCE AND REMOTE SENSING.